

Article

Efficient Power Management Strategy of Electric Vehicles Based Hybrid Renewable Energy

Naoui Mohamed ¹, Flah Aymen ¹, Ziad M. Ali ^{2,3}, Ahmed F. Zobaa ^{4,*} and Shady H. E. Abdel Aleem ⁵

¹ Processes, Energy, Environment and Electrical Systems (Code: LR18ES34), National Engineering School of Gabès, University of Gabès, Gabès 6072, Tunisia; mohamednaoui60@gmail.com (N.M.); aymen.flah@enig.u-gabes.tn (F.A.)

² Electrical Engineering Department, College of Engineering at Wadi Addawaser, Prince Sattam Bin Abdulaziz University, Wadi Addawaser 11991, Saudi Arabia; dr.ziad.elhalwany@aswu.edu.eg

³ Electrical Engineering Department, Aswan Faculty of Engineering, Aswan University, Aswan 81542, Egypt

⁴ Electronic and Computer Engineering Department, Brunel University London, Uxbridge UB8 3PH, UK

⁵ Department of Electrical Engineering, Valley High Institute of Engineering and Technology, Science Valley Academy, Qalubia 44971, Egypt; engyshady@ieeee.org

* Correspondence: azobaa@ieeee.org

Abstract: This paper presents a straightforward power management algorithm that supervises the contribution of more than one energy source for charging a vehicle, even if the car is in motion. The system is composed of a wireless charging system, photovoltaic (PV) generator, fuel cell (FC), and a battery system. It also contains a group of power converters associated with each energy resource to make the necessary adaptation between the input and output electrical signals. The boost converter relates to the PV/FC, and the boost-buck converter is connected with the battery pack. In this work, the wireless charging, FC, and PV systems are connected in parallel via a DC/DC converter for feeding the battery bank when the given energy is in excess. Therefore, for each of these elements, the mathematical model is formulated, then the corresponding power management loop is built, which presents the significant contribution of this paper. The efficient power management methodology proposed in this work was verified on Matlab/Simulink platforms. The battery state of charge and the hydrogen consumption obtained results were compared to show the effectiveness of this multi-source system.

Keywords: power management; renewable energy sources; electric vehicle; wireless charging system; photovoltaic generator; fuel cell generator



Citation: Mohamed, N.; Aymen, F.; Ali, Z.M.; Zobaa, A.F.; Abdel Aleem, S.H.E. Efficient Power Management Strategy of Electric Vehicles Based Hybrid Renewable Energy. *Sustainability* **2021**, *13*, 7351. <https://doi.org/10.3390/su13137351>

Academic Editor: Domenico Mazzeo

Received: 1 June 2021

Accepted: 27 June 2021

Published: 30 June 2021

Publisher's Note: MDPI stays neutral with regard to jurisdictional claims in published maps and institutional affiliations.



Copyright: © 2021 by the authors. Licensee MDPI, Basel, Switzerland. This article is an open access article distributed under the terms and conditions of the Creative Commons Attribution (CC BY) license (<https://creativecommons.org/licenses/by/4.0/>).

1. Introduction

Nowadays, the carbon dioxide rate has crossed 400 ppm, and it is still rising. Many solutions try to save the environment, and this is by finding some sustainable technologies that help reduce energy consumption or use some other energy resources. The car industry's interest in electrified powertrains is growing due to significantly reducing fuel consumption and harmful transportation emissions. The electrification of this main transport tool was studied as a severe challenge for having an efficient and robust transport tool. Therefore, researchers have not stopped improving in this field, providing many solutions and technical specifications for having a kind of electrified transport tool that is adaptable in use, and is safe and environmentally friendly.

Firstly, some solutions were concentrated on how it is possible using a pure electric vehicle (EV) or a hybrid electric vehicle (HEV). More than synthesis has tested these solutions and proves the advantages and drawbacks of each one. This study provides helpful information regarding the importance of EV or HEV and their problems [1]. These solutions were divided into more than a research field. Some of these studies were concentrated on the central traction part. The objective was to find the best electrical machine that can

be adapted inside an electric vehicle or inside a hybrid electric vehicle to increase the performance, minimize the vehicle weight, and have less energy consumed. The authors in [2] tested two kinds of machines adapted for HEV or EV and proved the importance of choosing the perfect machine in the traction part. On the other side, some applications were made on the power management solutions, and many reviews and studies were made. Some complicated solutions, based on intelligent controllers and others based on gaming theory, were found to be helpful, and these were evaluated by [3–5]. On the other side, the researchers were concentrated on how it is possible to increase vehicle autonomy. The given solution was also divided into more than one field [6]. Working on the battery technology or the recharge solutions was also profitable for improving the vehicle autonomy [7,8]. Other works were addressed to find a solution for reducing the recharge time or reducing the number of stops for recharge on a highway road [9,10]. The notion of fast recharge or grid notion to the vehicle is applied in the vehicle recharge field [11,12]. However, with another solution, the renewable energy field was also used for charging the vehicle, and the photovoltaic panels were used as an energy source for the recharge stations or for covering the vehicle body in order to extract the solar power and convert it to energy power inside the vehicle [13]. Additionally, the idea of a rechargeable road was defined recently, and the principle of wireless energy transmitter was found to be suitable for an electric vehicle on the road [14]. Some weaknesses were specified in this solution, as the vehicle speed cannot be high when using this solution. On the other side, the fuel cells method was also found helpful for a hybrid EV, and many research works were applied for testing this tool [15,16]. The only weakness of this kind of solution is the high noise, which can make the vehicle unconvertable. Additionally, some solutions based on regenerative braking systems were found valuable and helpful [17].

This study aims to combine the major of these recharge tools into the HEV and test the efficiency of the new combined recharge system. Using the photovoltaic, fuel cells, and the wireless transmitter will make the vehicle with a hybrid recharge system. These solutions significantly reduced the emission of radioactive elements that cause pollution of the environment and help to increase vehicle autonomy, mainly if used on highway roads.

Therefore, this paper is formulated to test the efficiency of a hybrid recharge tool based on multiple energy sources for charging the vehicle even if it is on the road. The combination of these recharge tools composes PV cells, FC generator, and a wireless recharge receiver to use the rechargeable induction roads.

This study provides a detailed mathematical exposition for each of these recharge solutions and exposes the corresponding power management loop, which can control the energetic flow from these sources to the main consumers: the motor or the main energy stock (the battery pack). The benefit of each energy recharge solution and the combination between them were investigated.

This paper is systematized as follows. After the previous Section 1, the hybrid electric vehicle composition is presented and discussed, and the interior architecture is shown in Section 2. In Section 3, the corresponding mechanical model and mathematical equations are formulated to explore the various forces acting on the vehicle body. Additionally, the traction system is described, and its related mathematical model is presented. The permanent magnet machine, its associated converter, and its primary energy source are introduced. The multi-source recharge tool is presented in Section 4. Firstly, the mathematical description for each energy source is formulated—the wireless energy transmitter, PV, and FC generators. The power management loop is presented at the end of this section. In Section 5, the simulation steps are carried out, and the results obtained are presented and discussed. A detailed discussion regarding the efficiency of this multiple recharge tool is introduced. In the end, the conclusion is given, and future endeavors are explored.

2. Composition of EVs

Hybrid electric vehicles (HEVs) have two or more sources of power onboard the vehicle and/or two or more sources of energy power [18,19]. This vehicle can be categorized into two categories: the first category is the pure EVs, and the second category is HEVs. This model provides electricity with some other source, in which the vehicle could be driven on a battery in an urban/populated area and could turn to the engine outside a city. Further, HEVs can be subdivided into plug-in HEVs (PHEVs) and fuel cell EVs (FCEVs). Thus, EVs may be classified into HEVs, battery-EVs (BEVs), PHEVs, and FCEVs [20]. The illustration of HEVs, addressed in this work, is shown in Figure 1.

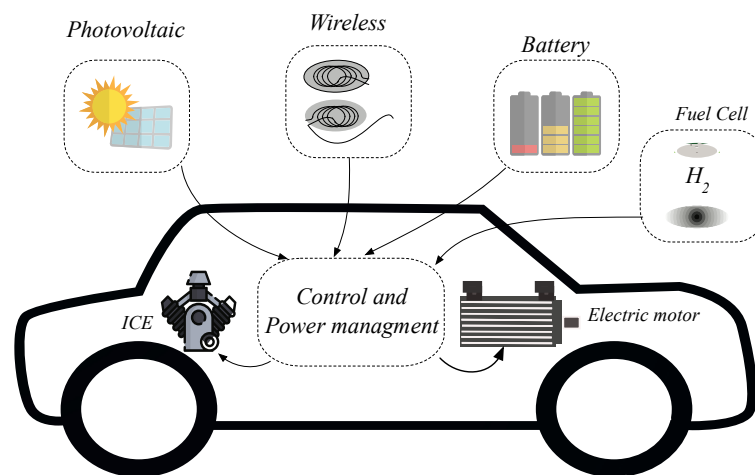


Figure 1. HEV model.

In the case of a battery charger for HEVs based on fuel cell energy, the amount of energy transferred depends on the energy source and vehicle composition, and the designer has to deal with particular points made by the system: wireless recharging (WR) system, PV generator, battery model, mechanical model, FC, electric motor, and buck-boost converter [21].

This paper proposes a multi-source system, and this system consists of FC system, a wireless charging system, a PV generator, and a lithium-ion battery. The system is shown in Figure 2.

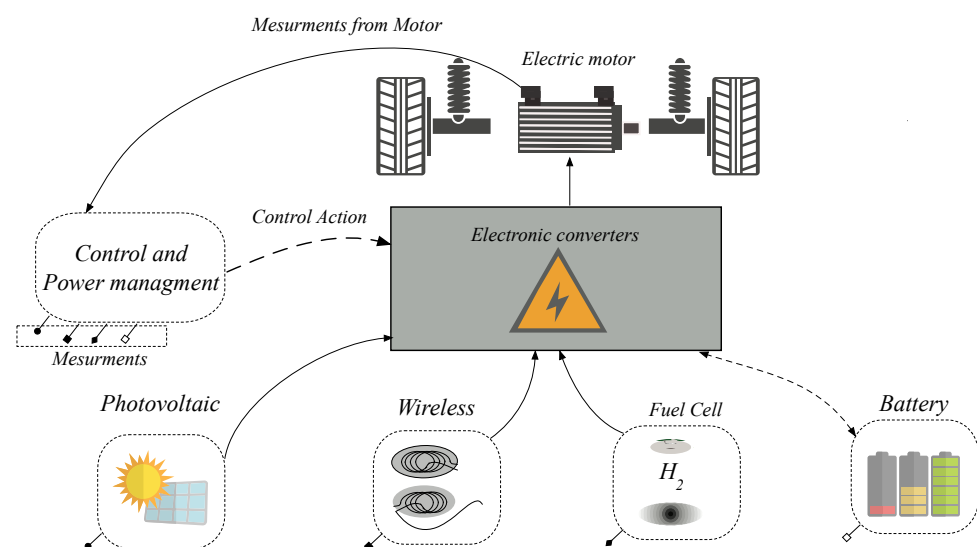


Figure 2. Architecture of the proposed multi-source system model.

3. The Vehicle Model

The comportment of a moving vehicle is determined by all the forces acting on it in that direction. Figure 3 illustrates the forces acting on the vehicle [22]. The tractive force F_t in the contact area between the tires of the drive wheels and the road surface thrusts the vehicle forward [23]. The torque from the power plant produces it and then transfers it through the transmission to the driving wheels. When the vehicle is mobile, there is resistance that attempts to stop its movement.

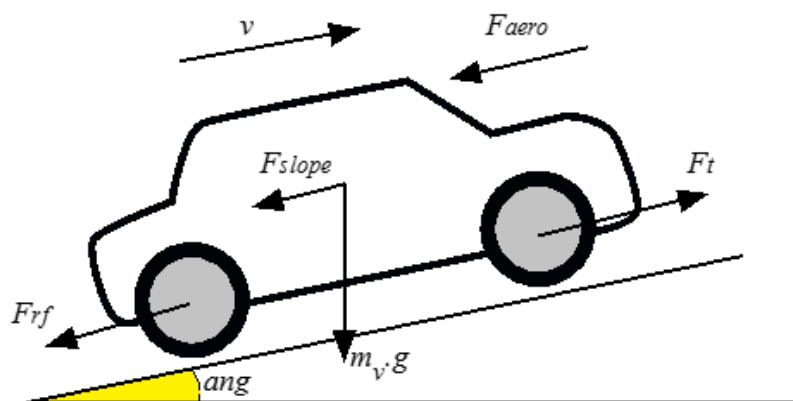


Figure 3. Schematic balance of forces acting on the vehicle.

3.1. Tractive Force

The mechanical model of the vehicle must make it possible to calculate the power necessary to propel the latter according to its characteristics, speed, and acceleration. To calculate the power required to move the vehicle forward, we apply the fundamental principle of dynamics [24,25].

$$\begin{cases} m_v d\vec{v}/dt = \sum \vec{F}_{ext}, \\ \sum \vec{F}_{ext} = \vec{F}_t - (\vec{F}_{rf} + \vec{F}_{slope} + \vec{F}_{aero}) \end{cases} \quad (1)$$

The force F_{aero} is equivalent to the aerodynamic drag force and is given by:

$$F_{aero} = \frac{1}{2} \rho_{air} v^2 A_f C_d \quad (2)$$

where ρ_{air} is the air density, v is the vehicle speed, A_f is the frontal vehicle area, and C_d is the aerodynamic drag coefficient.

The rolling resistance force of the wheels on the ground (F_{rf}) is given by the formula:

$$F_{rf} = C_r m_v g \cos(ang) \quad (3)$$

where C_r is the rolling resistance coefficient, g denotes the acceleration due to gravity, ang denotes the angle, and m_v is the vehicle mass.

The gravitational force (F_{slope}) depends on the road slope and is given as:

$$F_{slope} = m_v g \sin(ang) \quad (4)$$

The traction force expression (F_t) is represented as:

$$F_t = m_v \frac{dv}{dt} + F_{rf} + F_{slope} + F_{aero} \quad (5)$$

The mechanical power (P_m) required to move the vehicle forward is equal to the product of the traction force and the speed, thus:

$$P_m = F_t v \quad (6)$$

According to Equation (6), the load torque is given by:

$$T_r = F_r r \quad (7)$$

F_r is the total force and r is the tire radius.

3.2. Decomposition of the Traction System

3.2.1. Electrical Motor

The permanent magnet synchronous motor (PMSM) dynamic properties can be described by a set of nonlinear differential equations relating the stator and rotor currents and voltages with the mechanical quantities; torque, speed, and angular position [26–28]. After implementing Park transformation, the voltage expressions in the (d , q) axis are presented in Equation (8):

$$\begin{cases} v_d = R_s i_d + L_d \frac{di_d}{dt} - \omega L_q i_q \\ v_q = R_s i_q + L_q \frac{di_q}{dt} - \omega_m L_d i_d + \omega_m \lambda_m \end{cases} \quad (8)$$

where $v_d, v_q, i_d, i_q, L_d, L_q$ are the direct and the quadrature voltages, currents, and stator inductances, respectively. Additionally, ω_m denotes the mechanical speed of the electrical motor, and λ_m denotes the permanent magnet flux linkage. R_s is the stator resistance.

The electromechanical torque (T_e) can be represented as follows:

$$T_e = \frac{3}{2} \left(\frac{P}{2} \right) (\lambda_d i_q - \lambda_s i_d) \quad (9)$$

where $\lambda_d = L_d \cdot i_d + \lambda_m$ and $\lambda_q = L_q \cdot i_q$.

For the non-salient poles PMSM model, $L_d = L_q = L_s$, then the modified torque expression becomes:

$$T_e = \frac{3}{2} \left(\frac{P}{2} \right) (\lambda_m i_q) \quad (10)$$

The electromechanical motor equation is formulated as:

$$T_e - T_l = \frac{P_m}{2} \left(J \frac{d\omega_m}{dt} + f \omega_m \right) \quad (11)$$

where T_l, P_m and J denote the load torque, the number of poles, and the rotor inertia coefficient, respectively. The inverter voltage vector (\vec{V}_s) is given in (12):

$$\vec{V}_s = \sqrt{\frac{2}{3}} U_{DC} \left(S_a + S_b e^{i2\pi/3} + S_c e^{i4\pi/3} \right) \quad (12)$$

In this work, a PMSM of a maximum power of 50 kW was used. The parameters of this electric motor are summarized in Table 1.

Table 1. Parameters of the motor.

Parameters	Symbol	Values
Shaft power (w)	P_u	50,000
Pole pairs	P_m	2
Resistance of stator (Ω)	R_s	2.63
Resistance of rotor (Ω)	R_r	2.42
Mutual inductance (H)	M	0.253
Rotor and stator self-inductance (H)	$L_s = L_r$	0.214
Inertia moment (kgm^2)	J	0.03
Viscous friction (Nms^2)	f	0.0002

3.2.2. Battery Model

As the recharge system is employed to charge a battery pack, it is essential to recognize the mathematical battery model. The best performances can be found for the lithium model, and its detailed function can be visualized in [29,30]. In (13), we show the battery output voltage, referred to as ($V_{batt/cell}$) by one cell. Thus, the voltage expression depends on the (V_{oc}), which is the open-circuit voltage. R_{st} and C_{st} , which represent the resistance and capacitance of the electromagnetic short-term double-layer properties, respectively, and R_{lt} and C_{lt} , which represent the resistances and capacitances of the electro-chemical long-time-interval mass transport effects. As it can be discharged or charged, I_{st} could be either positive or negative.

$$V_{batt/cell} = V_{oc} + R_{batt}I_b + \int \frac{R_{lt}I_b - V_{lt}}{R_{lt}C_{lt}} dt + \int \frac{R_{st}I_b - V_{st}}{R_{st}C_{st}} dt \quad (13)$$

where R_{batt} and I_b denote the ohmic resistance and load current of the cell, respectively.

The battery pack voltage V_{batt} relies on the number of series (N_{sbatt}) and parallel (N_{pbatt}) cells used. Equation (14) formulates both V_{batt} and R_{batt} in terms of N_{sbatt} and N_{pbatt} .

$$\begin{cases} V_{batt} = \frac{N_{sbatt}}{N_{pbatt}} (V_{batt/cell}) \\ R_{batt} = \frac{N_{sbatt}}{N_{pbatt}} \left(R_o + R_{st} \left(\frac{I_{st}}{I_l} \right) + R_{lt} \left(\frac{I_{lt}}{I} \right) \right) \end{cases} \quad (14)$$

where R_o denotes the charging or discharging battery cell resistance.

The state of charge (SOC) of the battery can be expressed as a function of time as given in Equation (15) [31].

$$\begin{aligned} SOC(t) &= - \int_{t-1}^t \frac{1}{60} (SOC(t-1)N_b - W(V_b I_b)) dt \\ SOC(\%) &= \frac{Q(t)}{Q_{Max}} \times 100 \end{aligned} \quad (15)$$

where W denotes the charge/discharge coefficient, and N_b means the battery self-discharge.

3.2.3. Buck-Boost Converter

The battery is the main energy source connected to a two-quadrant DC/DC converter in this phase. This phenomenon is necessary as the storage system may have two different signs, positive or negative, allowing both directions to transfer energy. This converter has two roles—voltage elevation and minimization. A buck-boost DC converter assures this. The DC/DC converter comprises two IGBT transistors (S_1 and S_2) and a coil (L) connected, as illustrated in Figure 4.

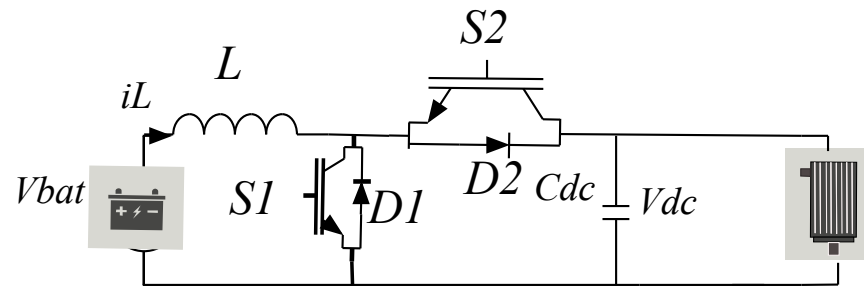


Figure 4. Bidirectional elevator chopper.

Steady-state converter analysis, the bidirectional converter works in boost when the switch S_1 and the diode D_2 are in conduction. In this case, the battery is discharged, and the current of the inductor i_L is positive. The mathematical model of the converter in boost mode is given by the differential system Equation (16).

$$\begin{aligned} \frac{di_L}{dt} &= -\frac{(1-u_1)}{L}V_{dc} + \frac{V_{bat}}{L} - \frac{R}{L}i_L \\ i_{bat} &= (1-u_1)i_L \end{aligned} \quad (16)$$

The bidirectional converter works in the buck mode when the switch S_2 and the diode D_1 are in conduction. In this case, the battery charges and i_L is negative. The mathematical model of the converter in buck mode is given by the differential system Equation (17).

$$\begin{aligned} \frac{di_L}{dt} &= -\frac{u_2}{L}V_{dc} + \frac{V_{bat}}{L} - \frac{R}{L}i_L \\ i_{bat} &= u_2i_L \end{aligned} \quad (17)$$

A binary variable Y is defined to represent the operating mode. Thus:

$$Y = \begin{cases} 1 & \text{si } i_{Lref} > 0 \quad (\text{boost}) \\ 0 & \text{si } i_{Lref} < 0 \quad (\text{buck}) \end{cases} \quad (18)$$

where i_{Lref} denotes the reference current to control S_1 and S_2 .

Hence, the converter (buck-boost) model can be obtained by:

$$\begin{aligned} \frac{di_L}{dt} &= -(Y(1-u_1) + (1-Y)u_2)\frac{V_{dc}}{L} + \frac{V_{bat}}{L} - \frac{R}{L}i_L \\ i_{bat} &= (Y(1-u_1) + (1-Y)u_2)i_L \end{aligned} \quad (19)$$

The control signal of the buck-boost converter, u_{12} , is defined and expressed by Equation (20).

$$u_{12} = Y(1-u_1) + (1-Y)u_2 \quad (20)$$

Therefore, the system of equations becomes:

$$\begin{aligned} \frac{di_L}{dt} &= -u_{12}\frac{V_{dc}}{L} + \frac{V_{bat}}{L} - \frac{R}{L}i_L \\ i_{bat} &= u_{12}i_L \end{aligned} \quad (21)$$

The DC bus of the system is modeled by a filter capacitor and is expressed in (22):

$$C_{dc} \frac{dV_{dc}}{dt} = i_1 + i_{bat} - i_{bus} \quad (22)$$

4. Hybrid Recharge System

This recharge system utilizes three kinds of energy sources: the wireless recharge model, PV panels, and FC generators. Therefore, modeling each of these facilities is essential to introduce this hybrid recharge tool clearly.

4.1. Wireless Power Transfer Model

The wireless charging device enables electrical energy to be transferred to the battery. An equivalent installation of the EV wireless charging device is shown in Figure 5a. The static model of the charger system with one receiver coil was studied in this section. In Figure 5b, a simplified representation of this inductive power transfer method is shown. V_S (secondary voltage) and V_P (primary voltage) represent this inductive power transfer's output and input voltages (IPT).

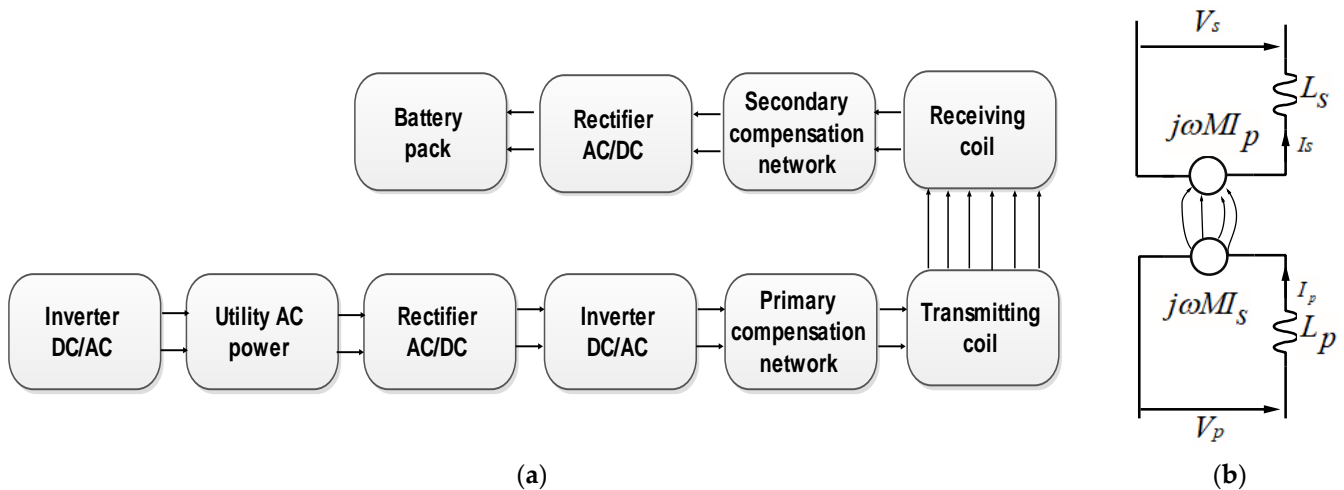


Figure 5. Recharge System: (a) Wireless charging system; (b) Simplified representation of wireless charging system.

The mutual inductance (M) is related to the magnetic coupling coefficient (k_{WR}) as follows, where L_p and L_s denote the primary and secondary inductances.

$$k_{WR} = \frac{M}{\sqrt{L_p L_s}} \quad (23)$$

The reflected impedance from the secondary to the primary is represented by:

$$Z_p = \frac{\omega^2 M^2}{Z_s} \quad (24)$$

ω denotes the oscillation angular frequency (rad/s). Additionally, Z_p and Z_s denote the primary and secondary impedances. Z_s depends on the selected compensation topology. The current I_s flows through the secondary winding is represented as follows:

$$I_s = \frac{j\omega M I_p}{Z_s} \quad (25)$$

The voltages across the primary and secondary windings are introduced as follows:

$$\begin{cases} V_p = j\omega L_p I_p - j\omega M I_s \\ V_s = j\omega M I_p - j\omega L_s I_s \end{cases} \quad (26)$$

The primary and secondary resonant frequencies are identical and given by:

$$\omega = \frac{1}{\sqrt{C_s L_s}} = \frac{1}{\sqrt{C_p L_p}} = 2\pi f \quad (27)$$

The power expressions (P_p and P_s) of the primary and secondary sides are expressed as follows:

$$\begin{aligned} P_p &= V_p I_p = (j\omega L_p I_p - j\omega M I_s) I_p \\ P_s &= V_s I_s = (j\omega M I_p - j\omega L_s I_s) I_s \end{aligned} \tag{28}$$

The power provided by the wireless charging system is proportional to the vehicle’s speed. This conclusion was previously proved in [31].

A wireless charging system of a maximum power of 8–10 kW is used in this work. The other parameters of the wireless charging system are summarized in Table 2.

Table 2. Wireless recharge system data.

Parameters	Values
i_1 (A)	20.0
U_{ref} (V)	480.0
Coil diameter (cm)	40.0
Distance between coils (cm)	140.0
Width of winding, W (cm)	19.0
Average winding radius, r (cm)	15.5
Number of turns, N (turns)	17.0

4.2. PV Generator Model

The solar cell is an electrical component used in some application requirements, such as an EV to transform solar energy into electricity to produce the electrical energy requirements. Many authors have suggested various models for modeling solar cells [32,33]. Figure 6 shows the single-diode model used to model the solar cell [34].

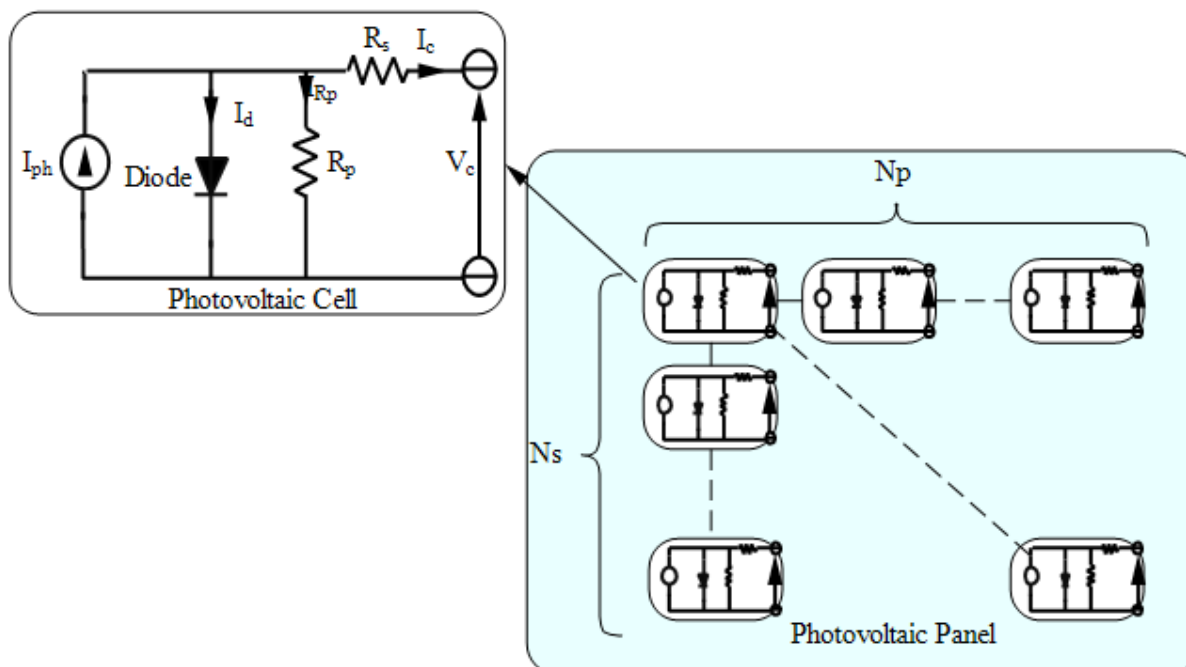


Figure 6. Equivalent model of a PV cell into a panel.

The current I_c is given by

$$I_c = I_{ph} + I_{sh} + I_d \tag{29}$$

The current I_{ph} (PV cell's current) can be evaluated as:

$$\begin{cases} I_{ph} = \frac{G}{G_{ref}} \left(I_{rs-ref} + \left[K_{SCT} (T_c - T_{c-ref}) \right] \right) \\ I_d = I_{rs} \left(e^{\frac{q(V_c + R_s I_c)}{akT}} - 1 \right) \\ I_{sh} = \frac{1}{R_p} (V_c + R_s I_c) \end{cases} \quad (30)$$

With I_{rs} current can be approximately obtained as:

$$I_{rs} = \frac{I_{rs-ref}}{e^{\left(\frac{qV_{oc}}{n_s * \eta \beta T_c} \right) - 1}} \quad (31)$$

Finally, the current I_c can be given by

$$I_c = I_{ph} - I_{rs} \left(e^{\left(\frac{q(V_c + R_s I_s)}{akT} \right) - 1} \right) - \frac{1}{R_p} (V_c + R_s I_s) \quad (32)$$

The model of a PV generator depends on the number of parallel and series cells, N_p and N_s . Finally, the PV generator current can be given by:

$$I_p = N_p I_{ph} - \left[N_p I_{rs} \left(e^{\left(\frac{q(V_c + R_s I_s)}{akT} \right) - 1} \right) - \frac{N_p}{R_p} \left(\frac{V_p}{n_s N_s} + \frac{R_s I_p}{N_p} \right) \right] \quad (33)$$

The parallel and series resistance (R_p and R_s) values are not be considered in this model, i.e., $R_p = \infty$ and $R_s = 0$. Thus:

$$I_p = N_p I_{ph} - \left[N_p I_{rs} \left(e^{\left(\frac{q(V_p)}{n \beta n_s T_c N_s} \right) - 1} \right) \right] \quad (34)$$

4.3. FC Generator Model

The FC uses air and hydrogen as fuel sources. Equation (35) shows the rates of conversion between the hydrogen $U_{f_{H_2}}$ and the oxygen $U_{f_{O_2}}$. Figure 7 shows the FC proton exchange membrane (PEM) [35].

$$\begin{cases} U_{f_{O_2}} = \frac{n_{o_2}^r}{n_{o_2}^m} = \frac{60,000 * R * T * i_{fc}}{2 * z * F * P_{air} * V_{air} * y\%} \\ U_{f_{H_2}} = \frac{n_{H_2}^r}{n_{H_2}^m} = \frac{60,000 * R * T * i_{fc}}{z * F * P_{fuel} * V_{fuel} * x\%} \end{cases} \quad (35)$$

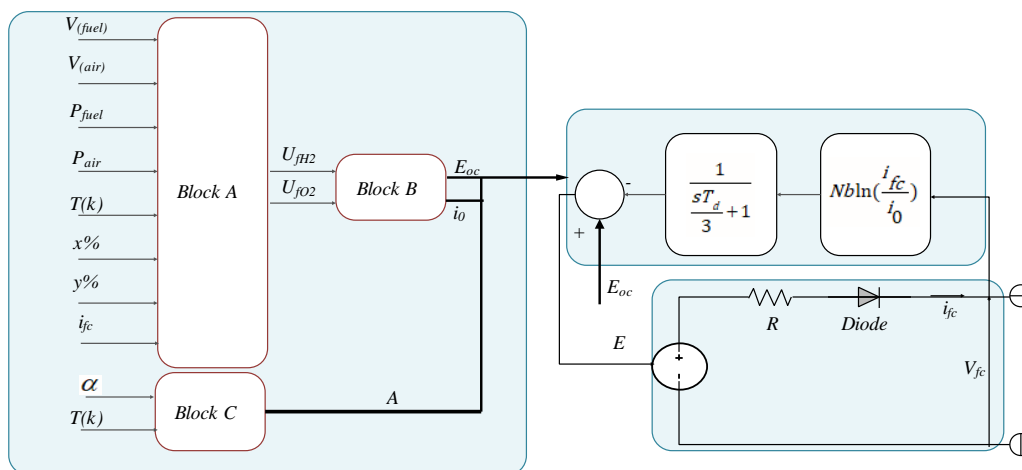


Figure 7. Equivalent circuit of the FC recharge tool.

The partial pressures of the hydrogen P_{H_2} , oxygen P_{O_2} and products water vapor defined by the parameters applied to block B, are expressed by the following equations [36]:

$$\begin{cases} P_{H_2} = (1 - U_{fH_2})x\%P_{fuel} \\ P_{H_2O} = (\omega_{fc} + 2y\%U_{fO_2})P_{air} \\ P_{O_2} = (1 - U_{fO_2})y\%P_{air} \end{cases} \quad (36)$$

where x denotes the hydrogen in the fuel (%) and y represents the oxygen in the oxidant (%).

When $T \leq 100$ °C

$$E_n = 1,229 + (T - 298) \frac{-44.43}{z * F} + \frac{R * T}{z * F} * \ln \left(P_{H_2} * P_{O_2}^{\frac{1}{2}} \right) \quad (37)$$

When $T > 100$ °C

$$E_n = 1,229 + (T - 298) * \frac{-44.43}{z * F} + \frac{R * T}{z * F} * \ln \left(\frac{P_{H_2} * P_{O_2}^{\frac{1}{2}}}{P_{H_2O}} \right) \quad (38)$$

Then, from the Nernst voltage (E_n) and the partial pressures of gases, the exchange current (i_0) and the values of the circuit voltage (E_{oc}) can be calculated as given in the following equations:

$$E_{oc} = K_c * E_n \quad (39)$$

$$i_0 = \frac{z * F * k * (P_{H_2} + P_{O_2})}{R h} e^{-(\Delta G / RT)} \quad (40)$$

Equation (41) expresses the Tafel slope model.

$$A = \frac{R * T}{z * \alpha * F} \quad (41)$$

Using the polarization curve at nominal operation conditions and some additional parameters, such as the stack efficiency, supply pressures, composition of fuel and air, and temperatures, the nominal rates of conversion gases can be estimated as it is in Equation (42).

$$\begin{cases} U_{fH_2} = \frac{\eta_{nom} * \Delta h_{(H_2O)g}^0 * N}{z * F * V_{nom}} \\ U_{fO_2} = \frac{60,000 * R * T_{nom} * N * I_{nom}}{2 * z * F * P_{airnom} * V_{1pm(air)nom} * 0.21} \end{cases} \quad (42)$$

The voltage source (E) can be given by

$$\begin{cases} E = E_{oc} - \left(N * A * \ln \left(\frac{i_{fc}}{i_0} \right) * \left(\frac{1}{1 + s T_d / 3} \right) \right) \\ V_{fc} = E - R_{fc} * i_{fc} \end{cases} \quad (43)$$

where i_{fc} is the FC current (A), R_{fc} is the internal resistance (Ω), N is the cells number, and T_d is the response time.

The expressions in Table 3 are used to calculate the detailed model parameters. The corresponding expression represents each variable.

Table 3. FC variables and their expressions.

Parameters	α	ΔG	K_c	K	K_1
Expression	$\frac{R * N * T_{nom}}{z * F * N * A}$	$-RT_{nom} * \ln \left(\frac{i_0}{K_1} \right)$	$\frac{E_{oc}}{E_{n(nom)}}$	$\frac{V_u}{K_c (U_{fO_2(max)} - U_{fO_2(nom)})}$	$\frac{2Fk(P_{H_2(nom)} + P_{O_2(nom)})}{hR}$

Where V_{fc} is the voltage of the FC (V), P_{fuel} is the pressure of fuel (atm), and P_{air} is the pressure of air (atm). K_c is the voltage of nominal operation conditions (V), z is the moving electrons, k is the Boltzmann's constant, and h is a constant (6.626×10^{-34} Js).

4.4. The Proposed Power Management Strategy

When the vehicle is in a garage or a covered parking place, the solar radiation cannot give the necessary power for starting the vehicle. Therefore, the battery/ultracapacitor is used for moving the vehicle. On the other hand, the battery charging method needs many technologies, solutions, or sources for quick recharge and increasing vehicle autonomy when it is on the highway [37]. Therefore, it is mandatory to control and supervise the different recharge solutions for improving the global efficiency of the battery [38].

An easy power management algorithm is built to show how to control the three used energy sources for charging the EV. The PV generator cannot be efficient only in particular weather conditions and vehicle positions, different from the dark zones or when the sunshine is covered. Therefore, the PV generator system is absent in this control algorithm when the vehicle starts from the stop position as a garage or covered parking. Even if the vehicle starts from a sunshine zone, the PV generator cannot collaborate by feeding the vehicle with the necessary energy, as its given power, not enough. Therefore, when the EV starts, the battery is used as the primary energy source. Next, if the EV is in motion, more than one case can occur, and this is related to the acceleration given ratio. Even the acceleration factor is high; the FC generator will contribute by the maximum as possible. Additionally, it is crucial to indicate that the wireless recharge method will decrease its contribution even the vehicle speed increase. The case of deceleration is also taken into account in this algorithm, and the idea is to shut down the FC generator. Therefore, based only on the wireless recharge method by percentage and according to the vehicle speed. The proposed algorithm is shown in Algorithm 1.

Algorithm 1. The proposed power management algorithm.

```

if (vehicle will start)
  {Battery is the main source of power (100% power from the battery)}
else if (vehicle is in motion)
  {Extract the maximum power from the PV generator (PV generator contribute by 100% in the
  energy sources)
    if (acceleration ratio is between 0 and 0.4%)
      - Use 10% of FC generator
      - Use 100% of power from the WR

    else if (acceleration ratio is between 0.4 and 0.6%)
      - Use 50% of FC power
      - Use 50% of WR power

    else (acceleration ratio > 0.6%)
      -Use 100% of power from the FC
      -Use 20% of WR power
  }
else if (Deceleration or Brake)
  {
    - FC is not used
    - WR power contribute by:
      { if (vehicle speed < 20 km/h)
        -Use all the power from the WR

        else if (20 km/h < vehicle speed < 40 km/h)
          -Use 50% of WR power
          else (40 km/h < vehicle speed)
            -Use 20% of WR power
      }
  }
  }
  
```

5. Results and Discussion

The simulation steps were carried out, and the results obtained are presented and discussed. A detailed discussion regarding the efficiency of this multiple recharge tool is introduced. However, it is necessary to mention that the presented results were obtained in the condition supposing each of these three-recharge systems is stable and running in the stationary mode. If one of these systems is not stable, the proposed solution will have difficulty, and the overall running system will need an adaptable control tool. The stability analysis and effects of each of these recharge tools are discussed in [39–41]. From the other side, investigation of the stability factors for each of these elements and on the global re-charge performance will be treated in our future endeavors.

5.1. Simulated Drive Cycle

The different simulation conditions were carried on after implementing the mathematical models on the Matlab/Simulink platform. The simulation time is calculated to have 300 m distance as a road. On this trajectory, there are 150 coils, and the distance between two coils is 1.5 m. Figure 8 shows this arrangement. On the other side, the car simulation model comprises 256 PV cells, which provide 6 kW electrical power in the best climatic conditions. The initial SOC of the battery is set to 65%.

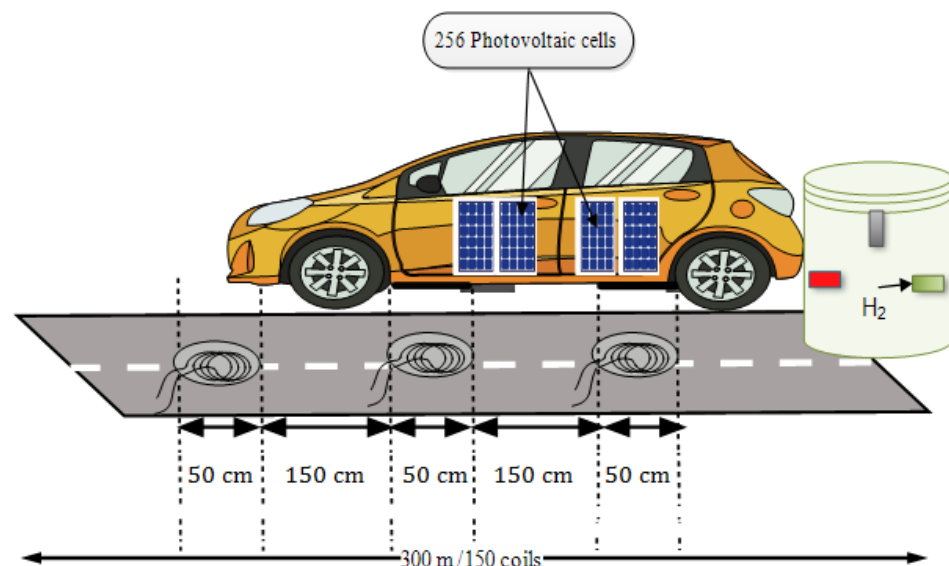


Figure 8. Road specification regarding the placement of the wireless recharge coils positions.

Values of the vehicle parameters and the electric motor used in the simulation are listed in Table 4.

Table 4. Parameters of the vehicle and the electric motor used in the simulation.

Parameter	Symbol	Value
Vehicle weight (kg)	m	20.0
Rolling resistance	f_r	480.0
Frontal surface area of the EV (m ²)	A_f	40.0
Tire radius (m)	R	140.0
Aerodynamic drag coefficient	C_d	19.0

In the different simulation steps, more than one parameter should be supervised and evaluated for calculating the efficiency of the power management algorithm. Essentially, the instant battery voltage, the battery state of charge, the instant battery current, the battery capacitor, and more need to be sensed and evaluated. These parameters

must be supervised for the measured vehicle speed and according to the given acceleration form. However, it is mandatory to oversee the energy flow of the different recharge sources and inspect the global energy management reaction.

Figure 9 shows the given driving cycle and the corresponding vehicle speed. It should be mentioned that the drive cycle form was applied for simulating a city road condition.

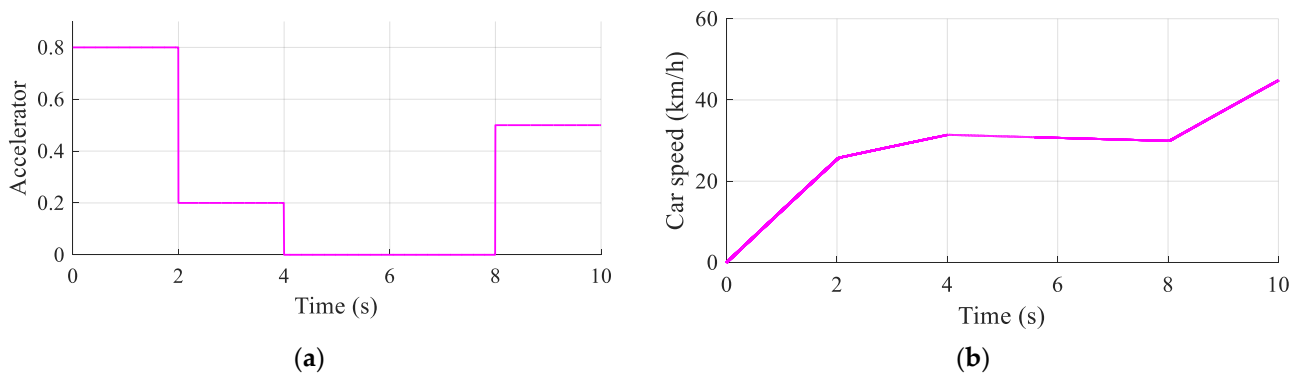


Figure 9. City road condition: (a) Accelerator; (b) speed.

According to the drive cycle, the profitability of the hybrid system can be verified, especially with supervising the battery's SOC. The forms of power delivered by the studied source are illustrated in Figure 10a–e for the power provided by the PV generator, wireless charging, FC generator, consumed power by the electric motor, and the battery power, respectively.

The implemented hybrid device provides enough power to drive the engine and charge the battery simultaneously, especially for low speeds, and this is shown in Figure 10e, between the instants 4 s and 8 s, where the given battery power is the minimum.

5.2. Hybrid System Efficiency

Figure 11 shows the SOC of the used battery. From the obtained results, it is possible to understand that the hybrid system runs perfectly, as indicated by the power management algorithm. Furthermore, to check the robustness of the hybrid system, a sudden shift in the rotational speed at $t = 2$ s, $t = 4$ s, and $t = 8$ s is made. The results obtained validate the hypothesis proposed. We note that even the induction motor's rotation speed varies, holding the flux steady. This figure shows that the SOC rate increases during weak acceleration, although the vehicle is in motion, and the same during the stop phase.

Figure 12 shows the dynamics of the consumption of hydrogen. It is clear that the hydrogen consumption rate is closely related to the power delivery by PV and WR systems. We note that the proposed hybrid system has contributed to saving a significant amount of hydrogen.

Based on this case of deceleration and brake mode, each recharge method was tested, and its energetic contribution can be evaluated. The best choice can be related to the combination between FC, PV, and WR. However, as the difference is not enough, the fundamental energy efficiency cannot be evaluated unless the PV weight system is correctly studied. It is demonstrated that with the new PV cells technology [42], the extra weight on the vehicle will be relatively affected. Therefore, one can conclude that the benefit of this renewable energy source is assured. However, it is also essential to indicate that the vehicle speed factor significantly influences the energetic performance as demonstrated in [2–5], which shows that PV cells and WR will contribute by 100% on a deceleration mode.

Finally, the efficiency of each recharge system can be summarized as presented in Table 5, in which this table classifies these recharge tools according to their energetic gain for the same road conditions.

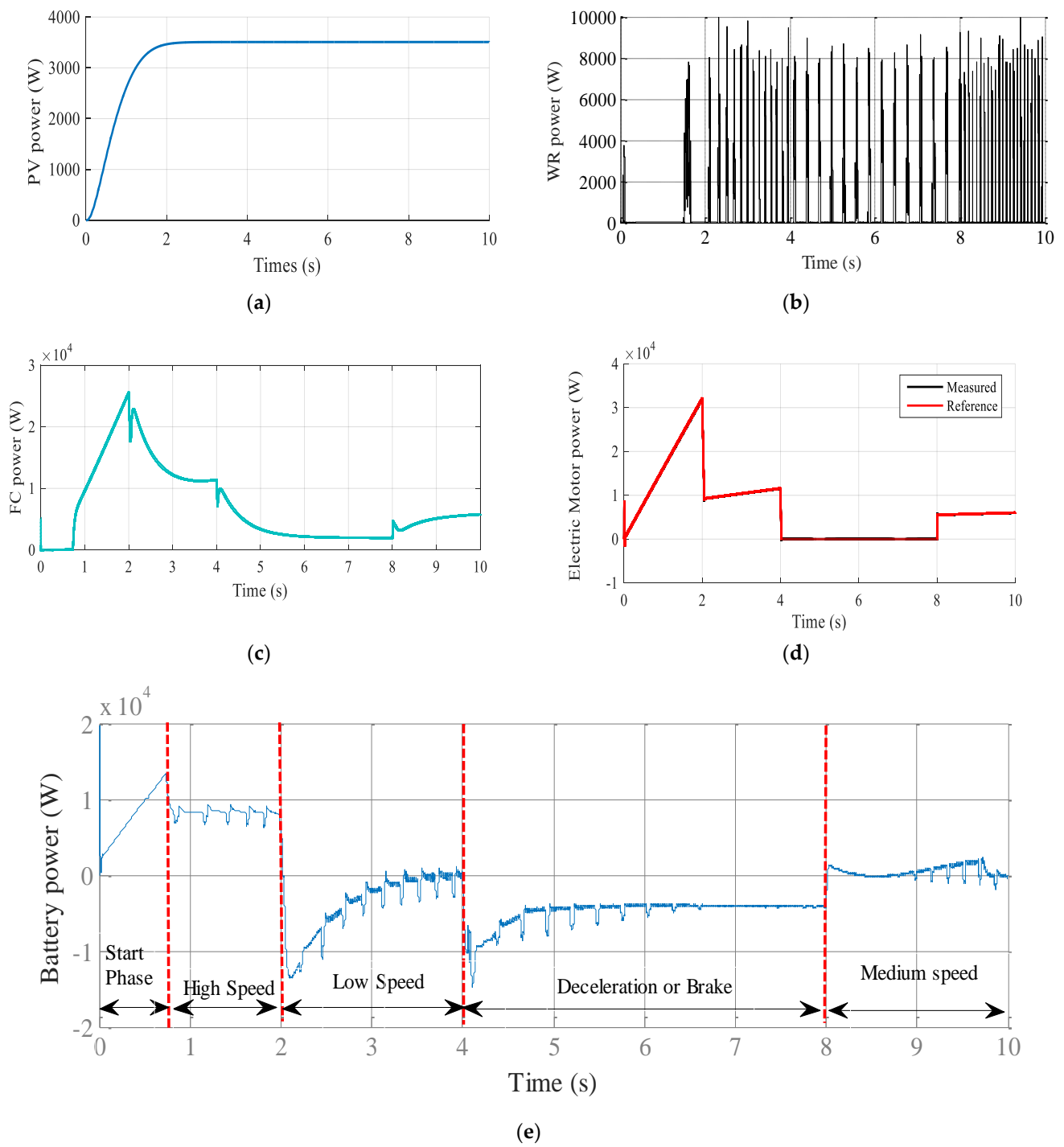
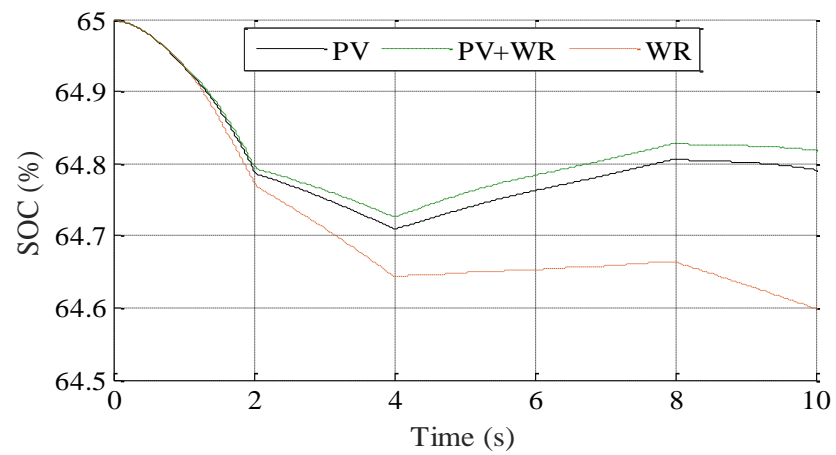
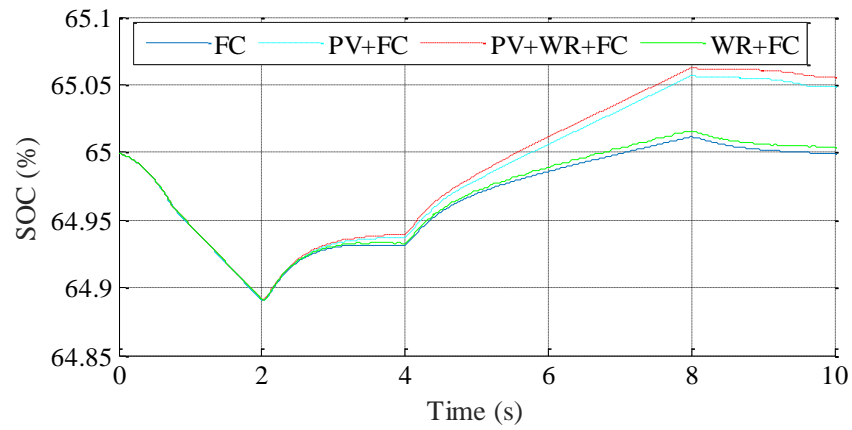


Figure 10. Results: (a) PV generator power; (b) wireless charging system power; (c) FC power; (d) consumed electric motor power; (e) battery power.



(a)



(b)

Figure 11. Battery state of charge: (a) without FC; (b) with FC.

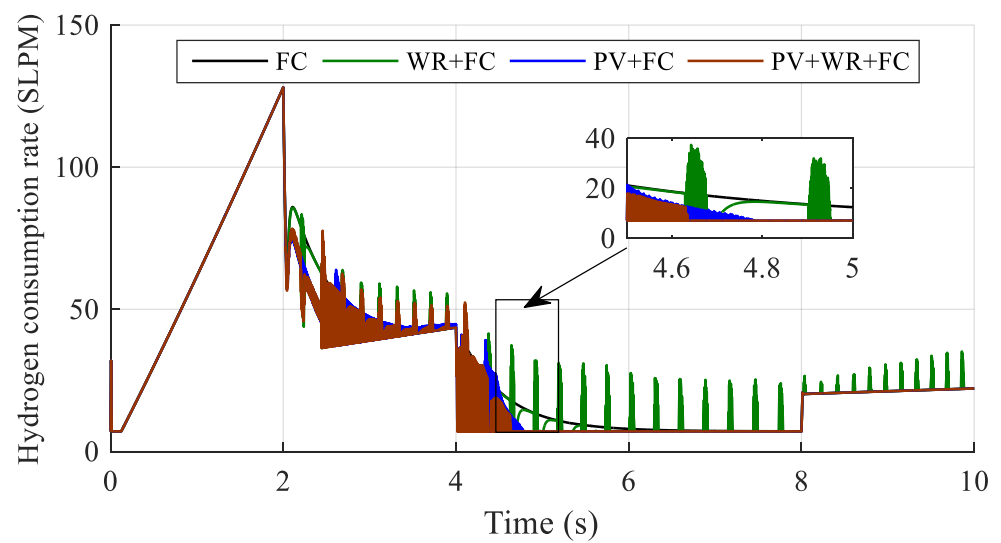


Figure 12. Dynamics of hydrogen consumption.

Table 5. Energetic contribution of the proposed multi-recharger system *.

Index/Metric	FC	PV+FC	WR+FC	PV+WR+FC
Energy gain	+	++	+	+++
Efficiency	+	++	+	+++
Renewable energy use	+	++	++	+++
Profitability	++	+++	++	+++

* In this table, + denotes low, ++ denotes moderate, and +++ denotes high.

6. Conclusions

This section ends the article after this report by outlining the key points and the main contribution of this study. Therefore, after providing all of the necessary equations for constructing a hybrid electric vehicle with a multi-charged source and displaying all of the internal models for the three studied recharge tools, a global model is designed and applied on the MATLAB Simulink tool to provide input on energy performance. The findings demonstrate that all of the designed models are operating well, and the power management control loop has been tested for the simulation test conditions. Statistics show that using this multi-recharge tool improves vehicle power performance and increases vehicle autonomy. However, some flaws in this analysis can be seen in terms of the weight of the PV recharge method and its global input on the real energetic gain. These flaws will only be fully evaluated if a thorough analysis of the PV weight system is conducted, which is why this issue is one of the work's future endeavors.

Author Contributions: F.A. and N.M. designed the problem under study; performed the simulations and obtained the results; Z.M.A., A.F.Z. and S.H.E.A.A. analyzed the obtained results; F.A. and N.M. wrote the paper, which was further reviewed by Z.M.A., A.F.Z. and S.H.E.A.A. All authors have read and agreed to the published version of the manuscript.

Funding: This research received no external funding.

Institutional Review Board Statement: Not applicable.

Informed Consent Statement: Not applicable.

Data Availability Statement: The data presented in this study are available on request from the corresponding author. The data are not publicly available due to their large size.

Conflicts of Interest: The authors declare no conflict of interest.

Nomenclature

ρ_{air}	Air density
C_d	Aerodynamic drag coefficient
C_r	Rolling resistance coefficient
v	Vehicle speed
A_f	Vehicle frontal area
m_v	Vehicle mass
g	Acceleration due to gravity
ang	Angle
R_s	Stator resistance
ω_m	Mechanical speed of the electrical motor
λ_m	Permanent magnet flux linkage
R_{batt}	Cell's ohmic resistance
I_b	Cell load current
R_o	Battery cell charging or discharging resistance
W	Charge/discharge coefficient
N_b	Stands of the battery self-discharge
SOC_{max}	Maximum state of charge
V_{fc}	Voltage of fuel cell (V)
P_{fuel}	Pressure of fuel (atm)

P_{air}	Pressure of air (atm)
V_{fuel}	Fuel flow rate (l/min)
V_{air}	Air flow rate (l/min)
N	Cells number
T_d	Response time
i_{fc}	Fuel cell current (A)
x	Hydrogen in the fuel (%)
y	Oxygen in the oxidant (%)
R_{fc}	Internal resistance (Ω)
z	Moving electrons
K_c	Voltage of nominal operation conditions (V)
k	Boltzmann's constant [J K ⁻¹]
η_{nom}	Nominal efficiency (%)
$\Delta h_{(H_2O)g}^0$	Enthalpy of water vapor (J mol ⁻¹)
V_{nom}	Nominal voltage (V)
I_{nom}	Nominal current (A)
P_{aimom}	Nominal absolute pressure of air (Pa)
Q	Battery capacity (Ah)
Q_{max}	Maximum Battery capacity (Ah)
SOC	State of charge (%)
T_{nom}	Nominal operating temperature (K)
P_{H_2O}	Water pressure (bar)
R	Constant (8.3145 J/(mol K))
h	Planck constant (6.626×10^{-34} J s)
α	Charge transfer coefficient
ω_{fc}	Percentage of water vapor %
M	Mutual inductance (H)
ω	Oscillation angular frequency (rad/s)
k_{WR}	Magnetic coupling constant
L_s	Secondary inductance (H)
L_p	Primary inductance (H)
Z_p	Primary impedance (Ω)
Z_s	Secondary impedance (Ω)
I_p	Primary current (A)
I_s	Secondary current (A)
V_p	Primary voltage (V)
V_s	Secondary voltage (V)

References

- Mahmoudi, C.; Flah, A.; Lassaad Sbita, P. An Overview of Electric Vehicle Concept and Power Management Strategies. In Proceedings of the 2014 International Conference on Electrical Sciences and Technologies in Maghreb (CISTEM), Tunis, Tunisia, 3–6 November 2014.
- Flah, A.; Irfan, A.K.; Agarwal, A.; Sbita, L.; Marcelo, G. simoes Field-oriented control strategy for double-stator single-rotor and double-rotor single-stator permanent magnet machine: Design and operation. *Comput. Electr. Eng.* **2021**, *90*, 1–15. [[CrossRef](#)]
- Kolmanovsky, I.; Dextreit, C. Approaches to energy management of hybrid electric vehicles: Experimental comparison. *J. Hydrol.* **2013**, *277*–282. [[CrossRef](#)]
- Mahmoudi, C.; Flah, A.; Sbita, L. Smart database concept for power management in an electrical vehicle. *Int. J. Power Electron. Drive Syst.* **2019**, *10*, 160–169. [[CrossRef](#)]
- Soltis, A.; Chen, X. A new control strategy for hybrid electric vehicles. In Proceedings of the 2003 American Control Conference, Denver, CO, USA, 4–6 June 2003; pp. 1398–1403. [[CrossRef](#)]
- Braune, S.; Liu, S.; Mercorelli, P. Design and control of an electromagnetic valve actuator. In Proceedings of the 2006 IEEE Conference on Computer Aided Control System Design, Control Applications, Intelligent Control, Munich, Germany, 4–6 October 2006; pp. 1657–1662.
- Kandasamy, K.; Vilathgamuwa, M.; Tseng, K.J. Inter-module state-of-charge balancing and fault-tolerant operation of cascaded H-bridge converter using multi-dimensional modulation for electric vehicle application. *IET Power Electron.* **2015**, *8*, 1912–1919. [[CrossRef](#)]
- Paganelli, G.; Tateno, M.; Brahma, A.; Rizzoni, G.; Guezennec, Y. Control development for a hybrid-electric sport-utility vehicle: Strategy, implementation and field test results. *IEEE Trans. Control Syst. Technol.* **2002**, *5064*–5069. [[CrossRef](#)]

9. Longo, M.; Zaninelli, D.; Viola, F.; Romano, P.; Miceli, R.; Caruso, M.; Pellitteri, F. Recharge stations: A review. In Proceedings of the 2016 Eleventh International Conference on Ecological Vehicles and Renewable Energies (EVER), Monte Carlo, Monaco, 6–8 April 2016; pp. 1–8.
10. Chellaswamy, C.; Ramesh, R. Future renewable energy option for recharging full electric vehicles. *Renew. Sustain. Energy Rev.* **2017**, *76*, 824–838. [[CrossRef](#)]
11. Tie, S.S.F.; Tan, C.W.C. A review of energy sources and energy management system in electric vehicles. *Renew Sustain Energy Rev.* **2013**, *20*, 82–102. [[CrossRef](#)]
12. Monteiro, V.; Pinto, J.G.; Afonso, J.L. Operation Modes for the Electric Vehicle in Smart Grids and Smart Homes: Present and Proposed Modes. *IEEE Trans. Veh. Technol.* **2016**, *65*, 1007–1020. [[CrossRef](#)]
13. Lawhorn, D.; Rallabandi, V.; Ionel, D.M. Power Electronics Powertrain Architectures for Hybrid and Solar Electric Airplanes with Distributed Propulsion. In Proceedings of the 2018 AIAA/IEEE Electric Aircraft Technologies Symposium (EATS), Cincinnati, OH, USA, 12–14 July 2018; pp. 1–6.
14. Werachet, K.; Heinz, Z. Wireless power charging on electric vehicles. In Proceedings of the International Electrical Engineering Congress, Pattaya, Thailand, 19–21 March 2014; pp. 6–9.
15. Cholakov, G.S. Electric vehicles. In *Pollution Control Technologies*; Nath, B., Cholakov, G.S., Eds.; Eolss Publishers: Oxford, UK, 2009; Available online: <http://www.eolss.net> (accessed on 24 May 2021).
16. Zandi, M.; Payman, A.; Martin, J.; Pierfederici, S.; Davat, B.; Meibody-Tabar, F. Energy Management of a Fuel Cell/Supercapacitor/Battery Power Source for Electric Vehicular Applications. *IEEE Trans. Veh. Technol.* **2011**, *60*, 433–443. [[CrossRef](#)]
17. Xu, L.; Hua, J.; Li, X.; Meng, Q.; Li, J.; Ouyang, M. Control strategy optimization of a hybrid fuel cell vehicle with braking energy regeneration. In Proceedings of the 2008 IEEE Vehicle Power and Propulsion Conference, Harbin, China, 3–5 September 2008.
18. Flah, A.; Majed, A.; Bajaj, M.; Naveen, K.S.; Mishra, S.; Sharma, S.K. Electric Vehicle Model Based on Multiple Recharge System and a Particular Traction Motor Conception. *IEEE Access* **2021**, *9*, 49308–49324. [[CrossRef](#)]
19. Rawat, T.; Niazi, K.R.; Gupta, N.; Sharma, S. Impact assessment of electric vehicle charging/discharging strategies on the operation management of grid accessible and remote microgrids. *Int. J. Energy Res.* **2019**, *43*, 9034–9048. [[CrossRef](#)]
20. Datta, U. A price-regulated electric vehicle charge-discharge strategy. *Energy Res.* **2019**, 1032–1042. [[CrossRef](#)]
21. Song, Z.; Hofmann, H.; Li, J.; Wang, Y.; Lu, D.; Ouyang, M.; Du, J. Torque Distribution Strategy for Multi-PMSM Applications and Optimal Acceleration Control for Four-Wheel-Drive Electric Vehicles. *J. Dyn. Syst. Meas. Control* **2020**, *142*. [[CrossRef](#)]
22. Miroslaw, T.; Szlagowski, J.; Zawadzki, A.; Zebrowski, Z. Simulation model of an off-road four-wheel-driven electric vehicle. *Proc. Inst. Mech. Eng. Part I J. Syst. Control Eng.* **2019**, *233*, 1248–1262. [[CrossRef](#)]
23. Minh, V.T.; Mohd Hashim, F.B.; Awang, M. Development of a real-time clutch transition strategy for a parallel hybrid electric vehicle. *Proc. Inst. Mech. Eng. Part I J. Syst. Control Eng.* **2012**, *226*, 188–203. [[CrossRef](#)]
24. Ye, J.; Huang, X.; Zhao, K.; Liu, Y. Optimal coordinating control for the overlapping shift of a seamless 2-speed transmission equipped in an electric vehicle. *Proc. Inst. Mech. Eng. Part I J. Syst. Control Eng.* **2017**, *231*, 797–811. [[CrossRef](#)]
25. Cunha, H.E.; Kyprianidis, K.G. Investigation of the Potential of Gas Turbines for Vehicular Applications. In Proceedings of the ASME Turbo Expo 2012: Turbine Technical Conference and Exposition, Copenhagen, Denmark, 11–15 June 2012; Volume 3, pp. 51–64.
26. An, Q.; Sun, L. On-line parameter identification for vector controlled PMSM drives using adaptive algorithm. In Proceedings of the 2008 IEEE Vehicle Power and Propulsion Conference, Harbin, China, 3–5 September 2008; pp. 8–13. [[CrossRef](#)]
27. Xu, J.; Wang, F.; Xie, S.; Xu, J.; Feng, J. A new control method for permanent magnet synchronous machines with observer. In Proceedings of the 2004 IEEE 35th Annual Power Electronics Specialists Conference, Aachen, Germany, 20–25 June 2004; Volume 2, pp. 1404–1408. [[CrossRef](#)]
28. Mercorelli, P. Parameters identification in a permanent magnet three-phase synchronous motor of a city-bus for an intelligent drive assistant. *Int. J. Model. Identif. Control* **2014**, *21*, 352–361. [[CrossRef](#)]
29. Tremblay, O.; Dessaint, L. Experimental Validation of a Battery Dynamic Model for EV Applications. *World Electr. Veh. J.* **2009**, *3*, 289–298. [[CrossRef](#)]
30. Rothenberger, M.J.; Safi, J.; Liu, J.; Anstrom, J.; Brennan, S.; Fathy, H.K. Improving Lithium-Ion Battery Pack Diagnostics by Optimizing the Internal Allocation of Demand Current for Parameter Identifiability. *J. Dyn. Syst. Meas. Control* **2017**, *139*. [[CrossRef](#)]
31. Mohamed, N.; Aymen, F.; Ben Hamed, M.; Lassaad, S. Analysis of battery-EV state of charge for a dynamic wireless charging system. *Energy Storage* **2019**, *5*. [[CrossRef](#)]
32. Mohamed, N.; Aymen, F.; Hamed, M. Ben Characteristic Of Photovoltaic Generator For The Electric Vehicle. *Int. J. Sci. Technol. Res.* **2019**, *8*, 871–876.
33. Mousa, A.G.E.; Abdel Aleem, S.H.E.; Ibrahim, A.M. Mathematical analysis of maximum power points and currents based maximum power point tracking in solar photovoltaic system: A solar powered water pump application. *Int. Rev. Electr. Eng.* **2016**, *11*, 97–108. [[CrossRef](#)]
34. Calasan, M.; Abdel Aleem, S.H.E.; Zobia, A.F. On the root mean square error (RMSE) calculation for parameter estimation of photovoltaic models: A novel exact analytical solution based on Lambert W function. *Energy Convers. Manag.* **2020**, *210*, 112716. [[CrossRef](#)]

35. Fathy, A.; Abdel Aleem, S.H.E.; Rezk, H. A novel approach for PEM fuel cell parameter estimation using LSHADE-EpSin optimization algorithm. *Int. J. Energy Res.* **2021**, *45*, 6922–6942. [[CrossRef](#)]
36. Hwang, J.J.; Chen, C.K.; Savinell, R.F.; Liu, C.C.; Wainright, J. A three-dimensional numerical simulation of the transport phenomena in the cathodic side of a PEMFC. *J. Appl. Electrochem.* **2004**, *34*, 217–224. [[CrossRef](#)]
37. Nentwig, M.; Mercorelli, P. Throttle valve control using an inverse local linear model tree based on a fuzzy neural network. In Proceedings of the 2008 7th IEEE International Conference on Cybernetic Intelligent Systems, London, UK, 9–10 September 2008; pp. 1–6.
38. Mostafa, M.H.; Aleem, S.H.E.A.; Ali, S.G.; Abdelaziz, A.Y.; Ribeiro, P.F.; Ali, Z.M. Robust energy management and economic analysis of microgrids considering different battery characteristics. *IEEE Access* **2020**, *8*, 54751–54775. [[CrossRef](#)]
39. Dharmakeerthi, C.H.; Mithulananthan, N.; Saha, T.K. Impact of electric vehicle fast charging on power system voltage stability. *Int. J. Electr. Power Energy Syst.* **2014**, *57*, 241–249. [[CrossRef](#)]
40. Wei, Z.; Peng, K.; Chen, J.; Yan, X.; Wan, Q. Stability Analysis of A DC Distribution System for Power System Integration of Plug-In Electric Vehicles. In Proceedings of the 2019 IEEE Innovative Smart Grid Technologies—Asia (ISGT Asia), Chengdu, China, 21–24 May 2019; Volume 5, pp. 2450–2455. [[CrossRef](#)]
41. Mandrile, F.; Cittanti, D.; Mallemaci, V.; Bojoi, R. Electric vehicle ultra-fast battery chargers: A boost for power system stability? *World Electr. Veh. J.* **2021**, *12*, 16. [[CrossRef](#)]
42. Sierra, A.; Reinders, A. Designing innovative solutions for solar-powered electric mobility applications. *Prog. Photovolt. Res. Appl.* **2020**, 1–17. [[CrossRef](#)]